

## PARAMETERISATION OF THE EDDY-EDDY AND EDDY-MEANFIELD INTERACTIONS IN THE LARGE EDDY SIMULATION OF OCEANIC CIRCULATIONS

**Vassili Kitsios**

Laboratory for Turbulence Research  
in Aerospace and Combustion,  
Mechanical Engineering Department,  
Monash University, Clayton, Australia.  
vassili.kitsios@monash.au

**Jorgen S. Frederiksen**

Centre for Australian Weather  
and Climate Research (CAWCR),  
CSIRO Marine and Atmospheric Research,  
Aspendale 3185, Victoria, Australia.  
jorgen.frederiksen@csiro.au

CAWCR, CSIRO Marine and Atmospheric Research,  
Aspendale 3185, Victoria, Australia.  
vassili.kitsios@csiro.au

**Meelis J. Zidikheri**

CAWCR, Bureau of Meteorology, Melbourne 3001, Victoria, Australia.  
m.zidikheri@bom.gov.au

### ABSTRACT

This paper presents parameterisations of the subgrid eddy-eddy and eddy-meanfield interactions in a baroclinic oceanic simulation representative of the Antarctic Circumpolar Current. High resolution benchmark simulations are undertaken using a quasi-geostrophic spectral spherical harmonic code of largest wavenumber  $T = 504$ . The eddy-eddy interactions are represented by both stochastic and deterministic parameterisations, with model coefficients determined from the benchmark simulation truncated back to the large eddy simulation (LES) truncation wavenumber  $T_R < T$ . Coefficients of the deterministic eddy-meanfield model are determined by a least squares regression method. Truncations are repeated for various  $T_R$ , with the dependence of the coefficients on the resolution  $T_R$  identified. Kinetic energy spectra from the LESs agree with the benchmark simulation. Scaling laws governing the subgrid coefficients are presented, which remove the need to generate the subgrid coefficients from benchmark simulations.

### INTRODUCTION

It is not possible to explicitly resolve all of the scales of motion in the ocean, so one resorts to large eddy simulation (LES), where the large eddies are resolved by a computational grid and the unresolved subgrid interactions are parameterised. In three-dimensional turbulence the empirical subgrid model of Smagorinsky (1963) is typically adopted, where the subgrid interactions are represented by an eddy viscosity. Here the eddy viscosity is given by a specified constant multiplied by a measure of the local grid size and the resolved strain rate. In simulations of two-dimensional and quasi-geostrophic (QG) turbulence, it is more appropriate for the eddy viscosity to be steeper in spectral space, taking the form of the Laplacian raised to a certain specified

power. Regardless of the method, if these interactions are not properly parameterised, then an increase in resolution will not necessarily increase the accuracy of the explicitly resolved scales. The dependence of the resolved scales on resolution has been an issue in general circulation models (GCMs) since the earliest studies, and persists today in even the most sophisticated GCMs (Koshyk & Hamilton, 2001).

There are four types of subgrid interactions: eddy-eddy; eddy-meanfield; eddy-topographic; and meanfield-meanfield (Frederiksen, 2012). The meanfield-meanfield type represent the interactions between the unresolved subgrid meanfield (time-averaged) and the resolved meanfield. The eddy-topographic form represents the interactions between the subgrid eddies and the resolved topography, and are more significant in regions of strong topographic features. Eddy-eddy interactions represent the impact unresolved subgrid eddies have on the evolution of the resolved eddies. The eddy-meanfield interactions represent the impact unresolved subgrid eddies have on the evolution of the resolved meanfield. The latter two interactions are the focus of the present study. In practice subgrid interactions in simulations of the ocean are represented by Redi (1982) and Gent & McWilliams (1990) type schemes, which respectively determine the diagonal and off-diagonal elements of the subgrid dissipation operator in isopycnal coordinates.

In the current paper parameterisations are presented for a flow representative of the Antarctic Circumpolar Current, simulated using a quasi-geostrophic spectral model. The spectral eddy viscosity coefficients are calculated from the statistics of high resolution benchmark numerical simulations truncated back to the desired LES truncation wavenumber. The coefficients representing the eddy-eddy and eddy-meanfield interactions are determined from the benchmark simulation using the processes of Frederiksen & Kepert (2006) and Kitsios *et al.* (2013b) respectively.

August 28 - 30, 2013 Poitiers, France

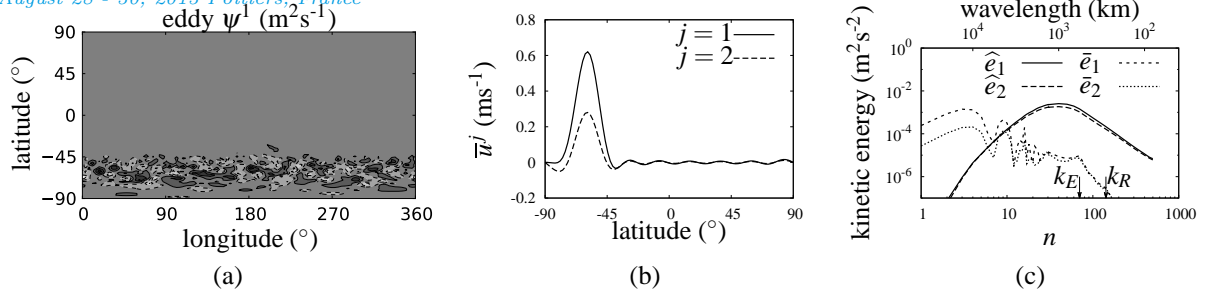


Figure 1. Benchmark simulation: (a) level 1 instantaneous non-zonal streamfunction ( $\psi^1$ ), with  $-1.4 \times 10^{-6} \text{m}^2 \text{s}^{-1}$  (black) to  $1.4 \times 10^{-6} \text{m}^2 \text{s}^{-1}$  (white); (b) time averaged zonal current ( $\bar{u}^j$ ); and (c) mean ( $\bar{e}_j$ ) and fluctuating ( $\hat{e}_j$ ) kinetic energy spectra.

## BENCHMARK SIMULATION

Flow fields are generated using the two-level QG model of Frederiksen (1998), which captures the essential dynamics of baroclinic and barotropic instabilities. The vorticity is represented at two vertical levels, with  $j = 1$  representing a depth of approximately 200m, and  $j = 2$  a depth of 600m. The system is nondimensionalised by using the radius of the Earth ( $a = 6371 \text{km}$ ) as a length scale, and the inverse of the Earth's angular velocity ( $\Omega = 7.292 \times 10^{-5} \text{s}^{-1}$ ) as a time scale. By default all variables are assumed to be non-dimensional unless units are specified.

The quasi-geostrophic potential vorticity equation (QGPVE) is spectrally discretised by expanding the field variables in spherical harmonics with the zonal (longitudinal) wavenumber  $m$ , and the total wavenumber  $n$ . This results in the prognostic equations for the spectral coefficients of the potential vorticity,  $q_{mn}^j = \zeta_{mn}^j + (-1)^j F_L [\psi_{mn}^1 - \psi_{mn}^2]$ , where the superscript  $j$  on the flow variables denotes the level,  $\zeta_{mn}^j = -n(n+1)\psi_{mn}^j$  are the spectral coefficients of the vorticity,  $\psi_{mn}^j$  the streamfunction coefficients, and  $n(n+1)$  is the discrete form of the Laplacian. Here  $F_L$  is a layer coupling parameter, related to the Rossby radius by  $r_R = 1/\sqrt{2F_L}$ . The evolution of  $q_{mn}^j$  is given by

$$\frac{\partial q_{mn}^j}{\partial t} = i \sum_{pq} \sum_{rs} K_{nqs}^{mpr} \psi_{-pq}^j q_{-rs}^j - i \omega_{mn} \zeta_{mn}^j - \alpha^j(n) \zeta_{mn}^j + \kappa_n (\bar{q}_{mn}^j - q_{mn}^j) - n(n+1) \sum_{l=1}^2 v_0^{jl}(m,n) q_{mn}^l. \quad (1)$$

The summations immediately after the equals sign are over the triangular wavenumber set  $\mathbf{T} = \mathbf{C}(T)$  where

$$\mathbf{C}(T) = [p, q, r, s \mid -T \leq p \leq T, |p| \leq q \leq T, -T \leq r \leq T, |r| \leq s \leq T], \quad (2)$$

and  $T$  is the benchmark simulation truncation wavenumber. The Rossby wave frequency is  $\omega_{mn} = -Bm/[n(n+1)]$ , where  $B = 2$  with the chosen nondimensionalisation. The drag at each level is given by the function  $\alpha^j(n) = \alpha_{max}^j [1 - \text{erf}(0.1(n-50))]/2$ , where  $\text{erf}$  is the error function, and  $\alpha_{max}^1 = 2.9 \times 10^{-7} \text{s}^{-1}$  and  $\alpha_{max}^2 = 1.2 \times 10^{-6} \text{s}^{-1}$ . The interaction coefficients  $K_{nqs}^{mpr}$  are detailed in Frederiksen and Kepert Frederiksen & Kepert (2006). All simulations are driven toward a mean state  $\bar{q}_{mn}^j$  that is purely zonal ( $\bar{q}_{mn}^j$  are zero unless  $m = 0$ ) and corresponds to a large-scale easterly current in the mid-latitudes of the southern hemisphere broadly representative of the ACC. The sim-

ulations are driven toward this state by a relaxation parameter  $\kappa_n$ , which for  $m = 0$  and  $n \leq 15$  has a value of  $\kappa_n = 10^{-6} \text{s}^{-1}$ , and  $\kappa_n = 0$  for all remaining wavenumber pairs. The bare eddy viscosity,  $v_0^{jl}(m,n)$ , is necessary as the benchmark simulation does not resolve all of the scales of motion. We represent  $v_0^{jl}(m,n)$  in its general anisotropic matrix form (dependent on  $m$  and  $n$ ) but in our simulations it is isotropic (dependent only on  $n$ ) where  $v_0^{jl}(m,n) = v_0^{jl}(n) = \delta_{lj} v_0^{jj}(T) [n/T]^{\rho_0^j - 2}$ , and  $\delta_{lj}$  is the Kronecker delta function, ensuring the off-diagonal elements are zero. Here  $v_0^{jj}(T)$  is the value of the diagonal elements at truncation and the exponent  $\rho_0^j$  determines the steepness of  $v_0^{jj}(n)$ . In all simulations we chose  $\mathbf{v}_0$  to have a form that would be consistent with it having been derived from a higher resolution benchmark simulation. Note there is no topography or orography in the present simulations.

In the present calculations  $T = 504$ , which is equivalent to 1536 longitudinal and 384 latitudinal grid points, or a grid point approximately every 0.238 degrees. The time step size used is  $\Delta t = 600 \text{s}$ , and the statistics are accumulated over a period of 6 years. The layer coupling parameter  $F_L = 2.5 \times 10^{-10} \text{m}^{-2}$ , corresponding to a Rossby radius of  $r_R = 1/\sqrt{2F_L} = 45 \text{km}$ . The non-dimensional Rossby wavenumber is  $k_R = a/r_R = 142$ , which is consistent with the simulations of Zidikheri & Frederiksen (2010).

A snapshot of the level 1 instantaneous streamfunction field ( $\psi^1$ ) minus the zonal component is shown in Fig. 1(a), which illustrates that the dominant structures are located in the mid to high latitudes of the southern hemisphere, consistent with the ACC. The corresponding time averaged zonal current ( $\bar{u}^j$ ) is shown as function of latitude in Fig. 1(b). The maximum velocity of the time averaged current at depths of 200m and 600m, are  $\approx 0.6 \text{ms}^{-1}$  and  $\approx 0.3 \text{ms}^{-1}$  respectively; consistent with measurements of the ACC in Phillips & Rintoul (2002). The kinetic energy spectra ( $e_j$ ) is decomposed into mean ( $\bar{e}_j$ ) and transient ( $\hat{e}_j$ ) energies. Figure 1(c) illustrates that the level 1 energy is greater than level 2 for all  $n$ . The energy containing scale wavenumber  $k_E \approx 70$  is defined as the extent of the flow configuration specific energy containing scales. This wavenumber is labelled on the  $n$  axis of 1(c) along with the Rossby wavenumber  $k_R$ . The phenomenological view of two-dimensional and QG turbulence is that energy and enstrophy are injected into the system via baroclinic instability at wavenumbers centred around  $k_R$ . There is an inverse energy cascade for the wavenumbers between  $k_E$  and  $k_R$ , and there is a forward enstrophy cascade for the wavenumber range past  $k_R$ . See Kitsios *et al.* (2013a) for further details on the basic flow.

## SUBGRID PARAMETERISATIONS

The resolution of a LES is lower than the associated benchmark simulation, and confined to the resolved scale wavenumber set  $\mathbf{R} = \mathbf{C}(T_R)$ , where  $T_R$  is the LES truncation wavenumber such that  $T_R < T$ . The subgrid wavenumber set is defined as  $\mathbf{S} = \mathbf{T} - \mathbf{R}$ . To facilitate a discussion on the flow decomposition, we let  $\mathbf{q} = (q_{mn}^1, q_{mn}^2)^T$  for a given wavenumber pair. In this vector notation  $\mathbf{q}_t(t) = \mathbf{q}_t^{\mathbf{R}}(t) + \mathbf{q}_t^{\mathbf{S}}(t)$ , where  $\mathbf{q}_t$  is the tendency (time derivative) of  $\mathbf{q}$ . The tendency of the resolved scales is  $\mathbf{q}_t^{\mathbf{R}}$ , where all triadic interactions involve wavenumbers less than  $T_R$ . The remaining subgrid tendency  $\mathbf{q}_t^{\mathbf{S}}$  has at least one wavenumber greater than  $T_R$  which is involved in the triadic interactions. One can further decompose  $\mathbf{q}_t^{\mathbf{S}}$  such that

$$\mathbf{q}_t^{\mathbf{S}}(t) = \widehat{\mathbf{q}}_t^{\mathbf{S}}(t) + \bar{\mathbf{f}}, \quad (3)$$

where  $\widehat{\mathbf{q}}_t^{\mathbf{S}}$  is the fluctuating component representing the eddy-eddy interactions, and  $\bar{\mathbf{f}} \equiv \langle \mathbf{q}_t^{\mathbf{S}} \rangle$  is the ensemble averaged subgrid tendency representing the eddy-meanfield interactions. The parameterisation of both of these interaction types are determined from the benchmark simulation.

### Subgrid eddy-eddy interactions

The  $\widehat{\mathbf{q}}_t^{\mathbf{S}}$  is represented by the stochastic equation

$$\widehat{\mathbf{q}}_t^{\mathbf{S}}(t) = -\mathbf{D}_d \widehat{\mathbf{q}}(t) + \widehat{\mathbf{f}}(t), \quad (4)$$

where  $\mathbf{D}_d$  is the subgrid drain dissipation matrix,  $\widehat{\mathbf{q}}$  is the fluctuating component of  $\mathbf{q}$ , and  $\widehat{\mathbf{f}}$  is a random forcing vector. As the present simulations have two vertical levels,  $\mathbf{D}_d$  is a time independent  $2 \times 2$  matrix, and  $\widehat{\mathbf{f}}$  is a time dependent 2 element column vector. The  $\mathbf{D}_d$  matrix is determined by post-multiplying both sides of (4) by  $\widehat{\mathbf{q}}^\dagger(t_0)$ , integrating over the decorrelation period  $\tau$ , ensemble averaging to remove the contribution of  $\widehat{\mathbf{f}}$ , and rearranging to produce

$$\mathbf{D}_d = - \left\langle \int_{t_0}^{t_0+\tau} \widehat{\mathbf{q}}_t^{\mathbf{S}}(\sigma) \widehat{\mathbf{q}}^\dagger(t_0) d\sigma \right\rangle \left\langle \int_{t_0}^{t_0+\tau} \widehat{\mathbf{q}}(\sigma) \widehat{\mathbf{q}}^\dagger(t_0) d\sigma \right\rangle^{-1} \quad (5)$$

where  $\dagger$  denotes the Hermitian conjugate for vectors and matrices. The angled brackets denote ensemble averaging, with each ensemble member determined by shifting  $t_0$  forward by one time step. The turbulence decorrelation time  $\tau$ , is chosen sufficiently large to capture the memory effects.

The model for  $\bar{\mathbf{f}}$  is determined by calculating the matrix  $\mathcal{F}_b = \mathbf{F}_b + \mathbf{F}_b^\dagger$ , where  $\mathbf{F}_b = \langle \widehat{\mathbf{f}}(t) \widehat{\mathbf{q}}^\dagger(t) \rangle$ . Post-multiplying both sides of (4) by  $\widehat{\mathbf{q}}^\dagger(t_0)$ , and adding the conjugate transpose of (4) pre-multiplied by  $\widehat{\mathbf{q}}(t_0)$  yields

$$\begin{aligned} & \left\langle \widehat{\mathbf{q}}_t^{\mathbf{S}}(t) \widehat{\mathbf{q}}^\dagger(t) \right\rangle + \left\langle \widehat{\mathbf{q}}(t) \widehat{\mathbf{q}}_t^{\mathbf{S}\dagger}(t) \right\rangle = \\ & -\mathbf{D}_d \left\langle \widehat{\mathbf{q}}(t) \widehat{\mathbf{q}}^\dagger(t) \right\rangle - \left\langle \widehat{\mathbf{q}}(t) \widehat{\mathbf{q}}^\dagger(t) \right\rangle \mathbf{D}_d^\dagger + \mathcal{F}_b. \quad (6) \end{aligned}$$

Given that  $\mathbf{D}_d$  is known,  $\mathcal{F}_b$  can now be calculated. At this point the formulation is general, and  $\widehat{\mathbf{f}}$  is coloured noise. For the implementation of the stochastic subgrid parameterisation, however, it is sufficient to assume that  $\widehat{\mathbf{f}}$  can be represented as the white noise process  $\langle \widehat{\mathbf{f}}(t) \widehat{\mathbf{f}}^\dagger(t') \rangle = \mathcal{F}_b \delta(t-t')$ .

The subgrid model in (4) represents this process in its fundamental stochastic form. One can also, however, represent the subgrid interactions using the simplified deterministic form  $\widehat{\mathbf{q}}_t^{\mathbf{S}}(t) = -\mathbf{D}_{\text{net}} \widehat{\mathbf{q}}(t)$ , where  $\mathbf{D}_{\text{net}}$  is the net dissipation representing the net effect of the drain and backscatter (Frederiksen & Kepert, 2006). The backscatter and net linear operators are defined by  $\mathbf{D}_b = -\mathbf{F}_b \langle \widehat{\mathbf{q}}(t) \widehat{\mathbf{q}}^\dagger(t) \rangle^{-1}$  and  $\mathbf{D}_{\text{net}} = \mathbf{D}_d + \mathbf{D}_b$  respectively (Frederiksen & Kepert, 2006). Theoretically the stochastic and deterministic methods are statistically equivalent.

The subgrid coefficients are presented in eddy viscosity form, where the drain, backscatter and net eddy viscosities are related to their respective dissipations by  $\mathbf{v}_d \equiv \mathbf{D}_d/[n(n+1)]$ ,  $\mathbf{v}_b \equiv \mathbf{D}_b/[n(n+1)]$ , and  $\mathbf{v}_{\text{net}} \equiv \mathbf{D}_{\text{net}}/[n(n+1)]$ , where  $n(n+1)$  is the discrete form of the Laplacian.

### Subgrid eddy-meanfield interactions

The parameterisation of the eddy-meanfield term represents the relationship between the ensemble averaged subgrid tendency  $\bar{\mathbf{f}}$ , and the ensemble averaged field  $\langle \mathbf{q} \rangle$ . For each wavenumber pair we assume the functional form

$$\bar{\mathbf{f}} = -\bar{\mathbf{D}} \langle \mathbf{q} \rangle + \mathbf{b}, \quad (7)$$

where  $\bar{\mathbf{D}}$  is a  $2 \times 2$  dissipation operator, and  $\mathbf{b}$  is a 2 element vector of constant coefficients. We assume that (7) also holds for small perturbations of the climate centred at the ensemble averaged climate, such that

$$\bar{\mathbf{f}}_i = -\bar{\mathbf{D}} \bar{\mathbf{q}}_i + \mathbf{b} + \boldsymbol{\varepsilon}_i, \quad (8)$$

where  $\bar{\mathbf{q}}_i$  and  $\bar{\mathbf{f}}_i$  are the time averaged meanfield and subgrid tendency calculated over the  $i$ -th non-overlapping time window of length  $\tau_M$ , and  $\boldsymbol{\varepsilon}_i$  is the associated 2 element error vector. The ensemble averages of each of the terms are  $\langle \bar{\mathbf{q}}_i \rangle \equiv \langle \mathbf{q} \rangle$ ,  $\langle \bar{\mathbf{f}}_i \rangle \equiv \bar{\mathbf{f}}$ , and  $\langle \boldsymbol{\varepsilon}_i \rangle = 0$ . The dissipation is solved for in a least squares sense, by subtracting (7) from (8), post-multiplying by  $(\bar{\mathbf{q}}_i - \langle \mathbf{q} \rangle)^\dagger$ , ensemble averaging both sides, and rearranging for  $\bar{\mathbf{D}}$  to produce

$$\bar{\mathbf{D}} = - \left( \langle \bar{\mathbf{f}}_i \bar{\mathbf{q}}_i^\dagger \rangle - \bar{\mathbf{f}} \langle \mathbf{q} \rangle^\dagger \right) \left( \langle \bar{\mathbf{q}}_i \bar{\mathbf{q}}_i^\dagger \rangle - \langle \mathbf{q} \rangle \langle \mathbf{q} \rangle^\dagger \right)^{-1}, \quad (9)$$

where we assume that the error term  $\boldsymbol{\varepsilon}_i$  is uncorrelated with  $(\bar{\mathbf{q}}_i - \langle \mathbf{q} \rangle)^\dagger$ . Once  $\bar{\mathbf{D}}$  is known we can determine the offset by rearranging (7) for  $\mathbf{b}$ . One can also present  $\bar{\mathbf{D}}$  scaled in eddy viscosity form,  $\bar{\mathbf{v}} \equiv \bar{\mathbf{D}}/[n(n+1)]$ .

### Implementation into large eddy simulations

The equations governing the LES are equivalent to those for the benchmark simulation, solved over the wavenumber set  $\mathbf{R}$  instead of  $\mathbf{T}$ , and with the addition of the subgrid tendency  $(q_t^{\mathbf{S}})_{mn}^j$ . The most general form of the subgrid tendency is the stochastic anisotropic representation

$$(q_t^{\mathbf{S}})_{mn}^j = - \sum_{l=1}^2 D_d^{jl}(m,n) \widehat{q}_{mn}^l + \widehat{f}_{mn}^j + \bar{f}_{mn}^j. \quad (10)$$

In the anisotropic deterministic form,  $D_d^{jl}(m,n)$  is replaced with  $D_{\text{net}}^{jl}(m,n)$ , and  $\widehat{f}_{mn}^j$  is removed. In the isotropic parameterisations the matrices  $\mathbf{D}_d$ ,  $\mathcal{F}_b$  and  $\mathbf{D}_{\text{net}}$  are isotropised, that is averaged over  $m$ .

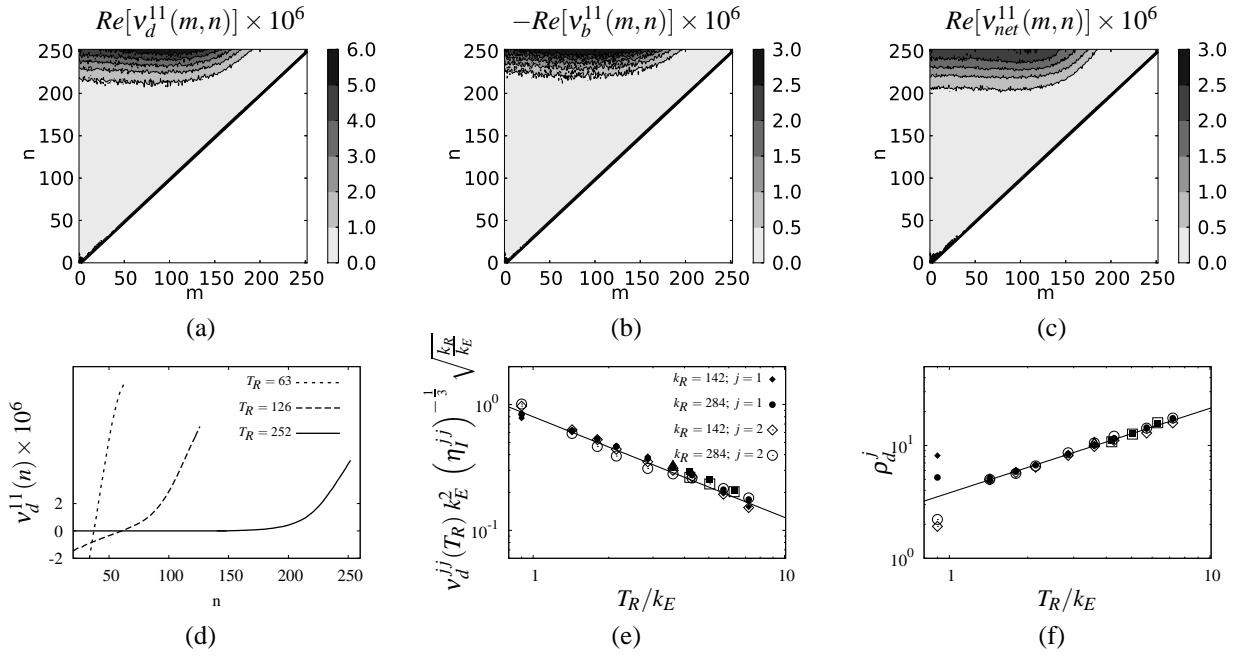


Figure 2. Eddy viscosity coefficients representing the eddy-eddy interactions. Anisotropic coefficients for  $T_R = 252$ : (a)  $Re[v_d^{11}(m,n)]$ ; (b)  $-Re[v_b^{11}(m,n)]$ ; and (c)  $Re[v_{net}^{11}(m,n)]$ . (d) Isotropic coefficients  $Re[v_d^{11}(n)]$  at various resolutions. Scaling laws for  $v_d^{11}(n)$ : (e) maximum value  $v_d^{11}(T_R)$ ; and (f) power exponent  $\rho_d^1(T_R)$

## SPECTRAL SUBGRID EDDY VISCOSITIES

In order to determine how the subgrid coefficients change with resolution, benchmark simulations are truncated back to various values of  $T_R$ . We first present the subgrid coefficients representative of the eddy-eddy interactions and then the eddy-meanfield interactions.

### Eddy-eddy coefficients

Firstly we present the anisotropic subgrid scale coefficients calculated from the benchmark simulation with  $T = 504$  truncated back to  $T_R = 252$ , with  $\tau = 288\Delta t = 2$  days. For each wavenumber pair, the dissipation operators  $\mathbf{D}_d$ ,  $\mathbf{D}_b$ , and  $\mathbf{D}_{net}$  are calculated and scaled into eddy viscosity form, with the real component of the upper diagonal elements  $v_d^{11}(m,n)$ ,  $-v_b^{11}(m,n)$ , and  $v_{net}^{11}(m,n)$  illustrated in Fig. 2(a), Fig. 2(b) and Fig. 2(c) respectively. The real components are the dominant terms, and we find that one can also run a LES with the imaginary components set to zero and closely replicate the kinetic energy spectra of the benchmark simulation. We plot the negative of  $v_b^{11}(m,n)$ , as this quantity is negative. Note the contour scale for each element is consistent with the relationship  $\mathbf{v}_d = -\mathbf{v}_b + \mathbf{v}_{net}$ . All of the eddy viscosities increase with  $n$ , have only a weak dependence on  $m$ , and hence are approximately isotropic. Although not illustrated, the lower diagonal element of the drain eddy viscosity  $v_d^{22}(m,n)$  is very similar in both form and magnitude to  $v_d^{11}(m,n)$ , and the off-diagonal elements  $v_d^{12}(m,n)$  and  $v_d^{21}(m,n)$  are small in comparison. At this resolution the drain eddy viscosity matrix is approximately isotropic and diagonal. The backscatter and net matrices also have these properties. These observations are consistent with the subgrid coefficients determined from atmospheric simulations in Kitsios *et al.* (2012). As we truncate to lower resolutions (lower values of  $T_R$ ), however, the subgrid coefficients become increasingly anisotropic and the off-diagonal elements become more significant (Kitsios *et al.*, 2013a).

To illustrate how these coefficients change with resolution, the isotropised upper diagonal element of the drain eddy viscosity ( $v_d^{11}(n)$ ) is illustrated in Fig. 2(d) for resolutions  $T_R = 252, 126$  and  $63$ . The  $T_R = 252$  case is the isotropised version of the coefficients in Fig. 2(a), and resides within the self-similar enstrophy cascading inertial range with  $k_R < T_R$ . The truncation at  $T_R = 126$  is within the inverse energy cascade as  $k_E < T_R < k_R$ . The final truncation at  $T_R = 63$  is within the non-self-similar energy containing scales as  $T_R < k_E$ . All of the profiles increase steeply as they approach  $T_R$ , and the maximum value as decreases as resolution increases. To further compress the information, the isotropised drain profiles are idealised by the function

$$v_d^{jj}(n) = v_d^{jj}(T_R) \left( \frac{n}{T_R} \right)^{\rho_d^j - 2}, \quad (11)$$

with the maximum value  $v_d^{jj}(T_R)$  and power exponent  $\rho_d^j$  determined through a least squares method. There are analogous expressions for the backscatter and net eddy viscosities. The diamonds symbols represent the simulations presented within having  $k_R = 142$  and  $k_E = 70$ , the circular symbols are for an alternate case with  $k_R = 284$  and  $k_E = 70$ , cases with  $k_R = 142$  and  $k_E \in (40, 50, 60)$  are represented by squares, and cases with  $k_R \in (201, 246)$  and  $k_E = 70$  are represented by triangles. For all cases, filled symbols represent  $j = 1$  and hollow symbols  $j = 2$ .

As illustrated in Fig. 2(f), when the wavenumbers are nondimensionalised by  $k_E$  the power exponents exhibit a strong relationship across the entire parameter space, with the steepness increasing as the truncation resolution increases. This is consistent with the discussion in Kraichnan (1976) which states that the distance the subgrid interactions can span in wavenumber space is determined by  $k_E$ . This wavenumber distance is represented by the width

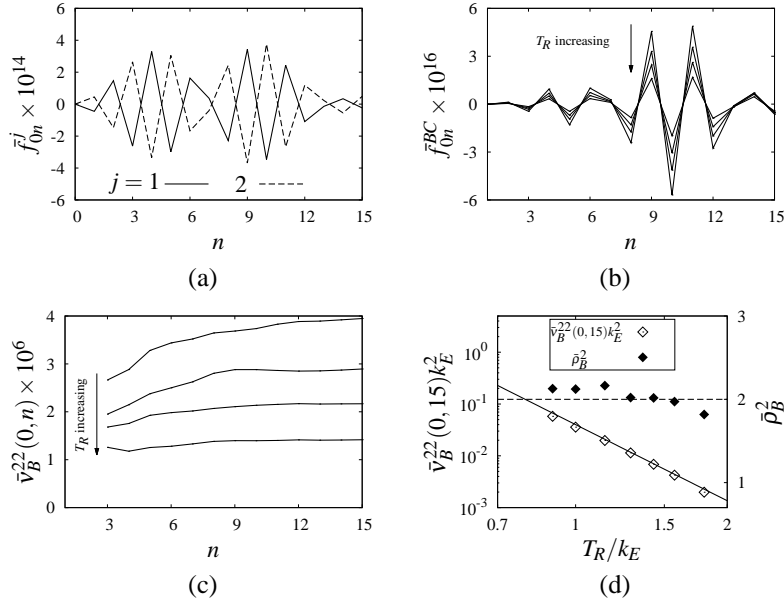


Figure 3. Subgrid eddy-meanfield parameterisation coefficients. (a) Mean potential vorticity tendency ( $\bar{f}_{0n}^j$ ) for an LES with  $T_R = 126$ . For  $T_R = 90, 100, 110, 120$  the: (b) mean baroclinic tendency ( $\bar{f}_{0n}^{BC}$ ); and (c) eddy viscosity component  $\bar{v}_B^{22}$ . (d) For various  $T_R$  the amplitude ( $\bar{v}_B^{22}(0, 15)$ ) and slope ( $\bar{\rho}_B^2$ ) of  $\bar{v}_B^{22}$  nondimensionalised by  $k_E$ .

of the eddy viscosity profiles, which is inversely proportional to the power exponents. As expected, only the truncations within the non-self-similar energy containing scales ( $T_R/k_E < 1$ ) do not follow the trend line. The scaling laws for the maximum values of the eddy viscosities are somewhat more complex and illustrated Fig. 2(e). We again use  $k_E$  to nondimensionalise all inverse length scales. In addition as outlined in Leith (1971), for a given  $k_E$  and  $k_R$ , the different values of  $v_d^{jj}(T_R)$  at each vertical level ( $j$ ) are collapsed by nondimensionalising the eddy viscosity using the time scale  $(\eta_l^{jj})^{-1/3}$ . An additional factor of  $\sqrt{k_R/k_E}$  is required, however, to span cases of different  $k_R$  and  $k_E$ . The results clearly illustrates that the eddy viscosities decrease in magnitude as resolution increases. The scaling laws for the exponents and magnitude of the drain, backscatter and net eddy viscosities can be found in Kitsios *et al.* (2013a).

### Eddy-meanfield coefficients

Long time integrations are required to calculate  $\bar{\mathbf{D}}$  as per (9), so the statistics are accumulated over a period of 100 years using a reference simulation with  $T = 252$ . The only mechanism for symmetry breaking in the equations of motion (1) is the forcing term  $\kappa_n(\bar{q}_{mn} - q_{mn})$ . As  $\kappa_n$  is only non-zero for  $m = 0$  and  $n \leq 15$ , it is only the values of  $\bar{f}_{mn}^j$  and  $\bar{q}_{mn}^j$  at these wavenumber components that should be non-zero under sufficient sampling. The average subgrid tendency is plotted in Fig. 3(a) for a truncation level  $T_R = 126$ , and we find that  $\bar{f}_{0n}^1$  is approximately a mirror image of  $\bar{f}_{0n}^2$ , having the effect of modifying the mean shear. This is true for all truncation levels. It therefore makes more sense to present  $\bar{\mathbf{f}}$  in baroclinic space where for each wavenumber pair  $\bar{\mathbf{f}}_B \equiv (\bar{f}_{mn}^{BT}, \bar{f}_{mn}^{BC})^T$ , with  $\bar{f}_{mn}^{BT}$  the barotropic component, and  $\bar{f}_{mn}^{BC}$  the baroclinic component which we find to be dominant for the present data. The transformation is given by  $\bar{\mathbf{f}}_B = \mathbf{B}\bar{\mathbf{f}}$ , where

$$\mathbf{B} = \frac{1}{2} \begin{bmatrix} 1 & 1 \\ \frac{1}{c_n} & -\frac{1}{c_n} \end{bmatrix}, \quad (12)$$

and  $c_n = 1 + 2F_L/[n(n+1)]$ . Subgrid truncations are repeated for lower values of  $T_R$ , with the dominant  $\bar{f}_{0n}^{BC}$  component illustrated in Fig. 3(b). As the system is truncated more heavily ( $T_R$  decreasing), there are more subgrid eddy-meanfield interactions and consequently  $\bar{f}_{0n}^{BC}$  increases. For various truncation levels we then calculate  $\bar{\mathbf{D}}$  using (9), and scale it into eddy viscosity units by  $\bar{\mathbf{v}} = \bar{\mathbf{D}}/[n(n+1)]$ . The eddy viscosity is then transformed into barotropic/baroclinic space via  $\bar{\mathbf{v}}_B = \mathbf{B}\bar{\mathbf{v}}$ . We find the  $\bar{v}_B^{22}$  component to be dominant, which represents the mean baroclinic tendency as a function of the mean baroclinic field. This component is plotted for various resolutions in Fig. 3(c), illustrating that as the truncation level decreases the required eddy viscosity increases, consistent with the observations of  $\bar{f}_{0n}^{BC}$ .

The change in magnitude ( $\bar{v}_B^{22}(0, 15)$ ) and slope ( $\bar{\rho}_B^2$ ) of the baroclinic eddy viscosity term is quantified by least squares fitting the  $\bar{v}_B^{22}(0, n)$  profiles to

$$\bar{v}_B^{22}(0, n) = \bar{v}_B^{22}(0, 15) [n/15]^{\bar{\rho}_B^2 - 2}, \quad (13)$$

for  $n \leq 15$ . These quantities are again nondimensionalised using  $k_E$  as an inverse length scale. We present data for the case with  $k_R = 142$  and  $k_E = 70$ . In Fig. 3(d),  $\bar{v}_B^{22}(0, 15)k_E^2$  are plotted as hollow diamonds on the left vertical axis against  $T_R/k_E$ , and the values of  $\bar{\rho}_B^2$  are plotted as filled diamonds on the right vertical axis. The steepness,  $\bar{\rho}_B^2$ , maintains a relatively constant value of approximately 2 for all  $T_R$ . The data also illustrates that as  $T_R$  increases (more scales resolved), the value of the strength  $\bar{v}_B^{22}(0, 15)$  decreases. The strength of the eddy-meanfield eddy viscosity also decreases with resolution much faster than the eddy viscosity representing the eddy-eddy interactions. This means that as the resolution increases, the eddy-meanfield interactions become proportionally less important. The eddy-meanfield eddy viscosities are also found to be insensitive to the choice of window period  $\tau_M$ , as long as  $\tau_M$  is greater than one week.

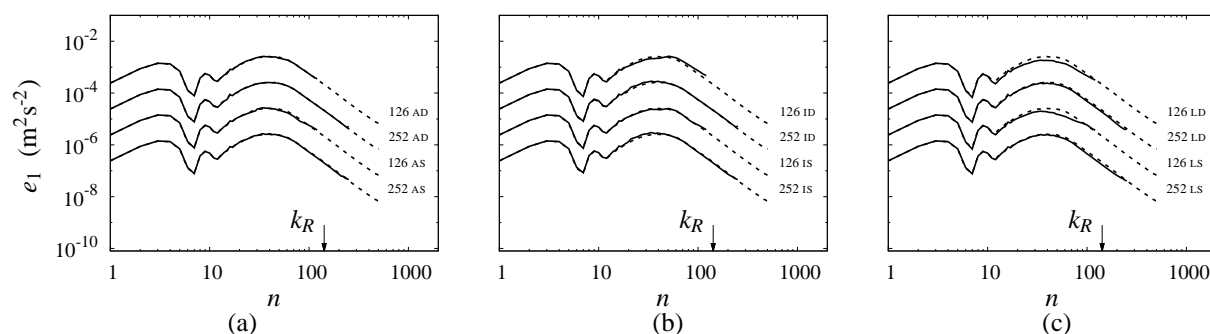


Figure 4. Spectra  $e_1$  (benchmark simulation - dashed, LES - solid) using parameterisations: (a) anisotropic deterministic (AD), stochastic (AS); and (b) isotropic deterministic (ID), stochastic (IS); and (c) isotropic scaling law deterministic (LD), stochastic (LS). Labelled with  $T_R$  and the associated subgrid parameterisation. The vertical axis in (a) is applicable to all figures.

## LARGE EDDY SIMULATION

We now incorporate the parameterisation for the eddy-eddy and eddy-meanfield interactions developed above into various LESs, as outlined in the discussion following (10). The spectra at level 1 ( $e_1$ ) for each of the LES variants with  $T_R = 126$  and  $252$  are compared to  $e_1$  of the benchmark simulation. The anisotropic deterministic and stochastic LES variants are compared to the benchmark simulation in Fig. 4(a), with each spectra offset for clarity. Both LES variants illustrate excellent agreement with the benchmark simulation. The isotropic deterministic and stochastic LES variants are compared to the benchmark simulation in Fig. 4(b), and again achieve excellent agreement. The idealised scaling law representation of the isotropic deterministic and stochastic LES variants are compared to the benchmark simulation in Fig. 4(c), and again achieve very good results. The drop in energy in the  $T_R = 126$  cases is due to the scaling laws not representing the negative component of the raw isotropic coefficients.

## CONCLUDING REMARKS

Subgrid parameterisations have been developed for the eddy-eddy and eddy-meanfield interactions for an oceanic circulation. The eddy-eddy interactions were represented by deterministic and stochastic subgrid parameterisations using the approach of Frederiksen & Kepert (2006). The stochastic variant consists of a drain eddy viscosity and a backscatter noise term, and the deterministic variant represents the net effect of the drain and backscatter. The eddy-meanfield interactions are represented using a deterministic method, with coefficients determined using the least squares approach of Kitsios *et al.* (2013b). In both approaches the wavenumber dependent eddy viscosity matrices have been derived from the statistics of higher resolution benchmark simulations. The kinetic energy spectra resulting from the LES agree with the spectra from the benchmark simulation.

## ACKNOWLEDGEMENTS

V. Kitsios acknowledges the CSIRO Office of the Chief Executive for funding this research project.

## REFERENCES

- Frederiksen, J. S. 1998 Precursors to blocking anomalies: the tangent linear and inverse problems. *J. Atmos. Sci.* **55**, 2419–2436.
- Frederiksen, J. S. 2012 Statistical dynamical closures and subgrid modeling for inhomogeneous QG and 3D turbulence. *Entropy* **14**, 32–57.
- Frederiksen, J. S. & Kepert, S. M. 2006 Dynamical subgrid-scale parameterizations from direct numerical simulations. *J. Atmos. Sci.* **63**, 3006–3019.
- Gent, P.R. & McWilliams, J.C. 1990 Isopycnal mixing in ocean circulation models. *J. Phys. Oceanogr.* **20**, 150–155.
- Kitsios, V., Frederiksen, J. S. & Zidikheri, M. J. 2012 Subgrid model with scaling laws for atmospheric simulations. *J. Atmos. Sci.* **69**, 1427–1445.
- Kitsios, V., Frederiksen, J. S. & Zidikheri, M. J. 2013a Scaling laws for parameterisations of subgrid eddy-eddy interactions in simulations of oceanic circulations. *Ocean Modelling* **in press**.
- Kitsios, V., Frederiksen, J. S. & Zidikheri, M. J. 2013b Subgrid parameterisation of the eddy-meanfield interactions in a baroclinic quasi-geostrophic ocean. *ANZIAM J.* **in press**.
- Koshyk, J.N. & Hamilton, K. 2001 The horizontal kinetic energy spectrum and spectral budget simulated by a high-resolution troposphere-stratosphere-mesosphere GCM. *J. Atmos. Sci.* **58**, 329–348.
- Kraichnan, R.H. 1976 Eddy viscosity in two and three dimensions. *J. Atmos. Sci.* **33**, 1521–1536.
- Leith, C. E. 1971 Atmospheric predictability and two-dimensional turbulence. *J. Atmos. Sci.* **28**, 145–161.
- Phillips, H.E. & Rintoul, S.R. 2002 A mean synoptic view of the subantarctic front south of Australia. *J. Phys. Oceanogr.* **32**, 1536–1553.
- Redi, M.H. 1982 Oceanic isopycnal mixing by coordinate rotation. *J. Phys. Oceanogr.* **12**, 1154–1158.
- Smagorinsky, J. 1963 General circulation experiments with the primitive equations: I. the basic experiment. *Mon. Wea. Rev.* **91** (3), 99–164.
- Zidikheri, M. J. & Frederiksen, J. S. 2010 Stochastic modelling of unresolved eddy fluxes. *Geophysical and Astrophysical Fluid Dynamics* **104**, 323–348.